GOSPODARKA SUROWCAMI MINERALNYMI – MINERAL RESOURCES MANAGEMENT

2026 Volume 42 Issue 3 Pages 67–84

DOI: 10.24425/gsm.2026.6004

SEBASTIAN PREWENDOWSKI[1], WOJCIECH PANNA[2], MAGDALENA SZUMERA[3], SEBASTIAN KOMAREK[4], PIOTR STĘPIEŃ[5]

# Pozzolanic reactivity and specific surface area of thermally treated clay materials: comparative study of smectite, illite and kaolinite-based compositions

## Introduction

The specific surface area of clay raw materials is one of the key parameters influencing their physical and chemical properties. The magnitude of the specific surface area largely depends on the phase composition of the raw materials and the degree of crystallinity of the mineral components (Dondi et al. 1998), as well as preliminary processing, microporosity, and exchangeable cations (in smectites) (Kaufhold et al. 2010). A significant content of clay minerals – particularly smectite group minerals and halloysite – accounts for a high

✉ Corresponding Author: Sebastian Prewendowski; e-mail: prewendo@agh.edu.pl
[1] AGH University of Krakow, Poland; ORCID iD: 0000-0002-2307-5588; e-mail: prewendo@agh.edu.pl
[2] University of Applied Sciences in Tarnow, Poland; ORCID iD: 0000-0002-6591-284X; e-mail: w_panna@atar.edu.pl
[3] AGH University of Krakow, Poland; ORCID iD: 0000-0002-5692-8161; e-mail: mszumera@agh.edu.pl
[4] AGH University of Krakow, Poland: ORCID iD: 0000-0002-3002-8421; e-mail: seko@agh.edu.pl
[5] AGH University of Krakow, Poland: ORCID iD: 0000-0001-7340-6704; e-mail: pstepien@agh.edu.pl

specific surface area (Wyszomirski et al. 2024). These results, among other factors, result from the crystallization conditions of clay minerals, which are often subject to isomorphic substitutions within their structure (Wang et al. 2017).

Clay raw materials can be divided into the serpentine–kaolin group, micas, smectites, vermiculites, and chlorites (Bergaya and Lagaly 2013). The main clay minerals occurring in these raw materials are kaolinite, montmorillonite, illite, chlorite, and vermiculite (Carroll 1970; Bergaya and Lagaly 2013). Kaolinite is a 1:1 type mineral (Figure 1), forming layers bonded together by hydrogen bonds (Brigatti et al. 2013). This structure results in kaolinite having a lower specific surface area and lower water absorption (Kuila and Prasad 2013). Illite has a three-layer structure like mica, where layers are held together by potassium ions, giving it higher plasticity and specific surface area than kaolinite (Murray 2006). Smectite, characterized by its three-layer structure (Figure 1), exhibits high swelling capacity and specific surface area (Murray 2006; Brigatti et al. 2013). The type of smectite is also important – $Ca^{2+}$- and $Mg^{2+}$-smectites generally show higher BET specific surface area compared to $Na^{+}$-smectites, which results from differences in the hydration of exchangeable cations. In contrast, $Na^{+}$-smectites typically exhibit higher swelling capacity than their $Ca^{2+}$ and $Mg^{2+}$ counterparts (Ayari et al. 2007; Kaufhold et al. 2010).

The specific surface area of clay raw materials also depends on their particle size distribution, which is reflected in grain size distribution diagrams (Dogan et al. 2006;

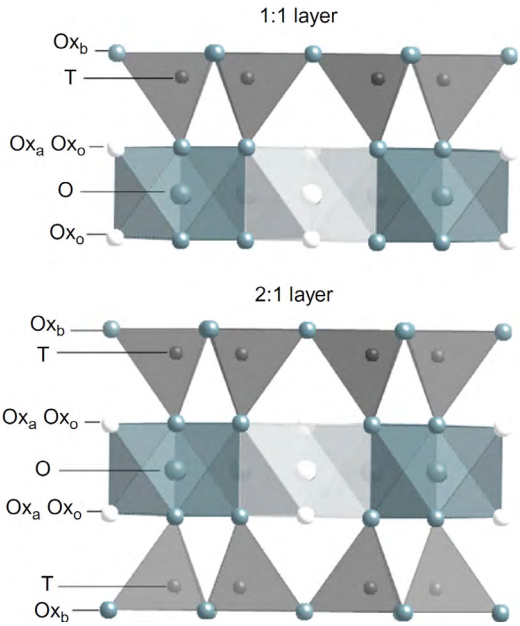


Fig. 1. Models of 1:1 and 2:1 layer structures
$Ox_b$ – basal oxygen atoms, T – tetrahedral cations, O – octahedral cations,
$Ox_a$ – apical oxygen atoms, $Ox_o$ – octahedral anions (OH, F, Cl) 7 (Brigatti et al. 2013)

Rys. 1. Modele struktur warstwowych w skali 1:1 i 2:1

Dogan et al. 2007). Fractions below 2 µm correspond to the presence of clay minerals (Schulze 2005; Tan et al. 2017). Stoch and Sikora (1971) showed that minerals in plastic clay rocks exhibit characteristic grain size ranges (Figure 2). The finest-grained bentonites, composed mainly of smectite, reach specific surface areas up to 800 $m^2/g$ (Irawan and Samsuri 2006). Such materials display exceptional sorptive, plasticizing, rheological (Wang et al. 2017; Xie et al. 2024; Panna et al. 2025) and catalytic activity (Schoonheydt and Johnston 2011). They are used as sorptive materials in hazardous waste landfill liners, as sorbents for removing heavy metals and pollutants (Koch 2002; Wyszomirski et al. 2024) and in the production of lightweight aggregates (Panna et al. 2024).

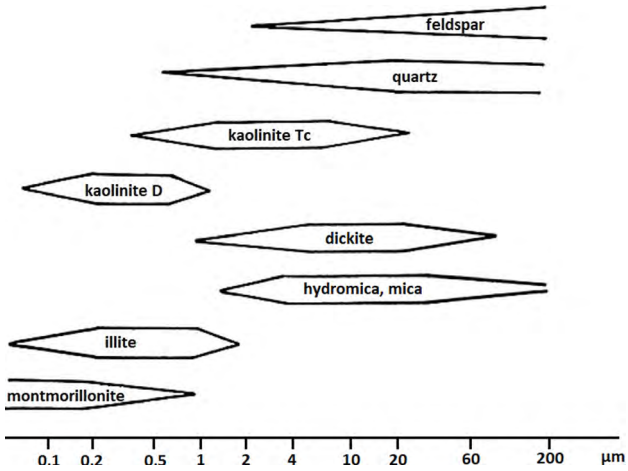


Fig. 2. Characteristic grain size ranges of some clay minerals (Stoch and Sikora 1971)

Rys. 2. Charakterystyczne przedziały wielkości ziaren niektórych minerałów ilastych

Clay raw materials with a highly developed surface area are rarely subjected to thermal treatment, since an excess of smectite or other fine-grained minerals may cause drying difficulties and cracking in finished products (Koch 2002). Mineralogical characteristics, including the type, stability, and quantity of clay minerals, as well as impurities, are crucial (Hollanders 2017). Pozzolanic materials – classified as SCMs (supplementary cementitious materials) – can react with water and lime, producing hardened materials with improved strength (Liu et al. 2021). The most well-known natural pozzolans include materials such as perlite and zeolite, while metakaolin and silica fume are considered artificial pozzolans obtained through thermal or industrial processes (Amiri et al. 2022). Producing one mass unit of metakaolinite requires about 80% less heat than cement (Lech and Wyszomirski 2020). Reducing clinker content by replacing it with SCMs is a promising way to lower the carbon footprint of the cement industry, as their production generates far fewer $CO_2$ emissions than Portland cement, which accounts for about 8% of anthropogenic $CO_2$ emissions (Zunino and Scrivener 2024).

Metakaolinite is formed through the dehydroxylation of kaolinite during thermal treatment (Bellotto et al. 1995). The temperature and duration of calcination significantly influence its pozzolanic activity, which also depends on kaolinite structure, impurities, and particle size (Liu et al. 2021). Dehydroxylation begins near 550°C (Daou et al. 2023); disordered kaolinite dehydroxylates between 530–570°C, and ordered between 570–630°C. The disordered form shows higher pozzolanic activity (Kakali et al. 2001). Thermogravimetric and calorimetric analyses confirm that hydroxyl release starts at 550°C. Most researchers identify the optimal calcination range as 650–850°C, most commonly 650–750°C (Snellings et al. 2012; Rashad 2013). Above 900°C, metakaolinite sinters and transforms into stable crystalline phases, such as spinel-type structures, losing their pozzolanic properties (Lech and Wyszomirski 2020; Liu et al. 2021). The formation of metakaolinite during the thermal treatment of kaolinite involves the breakdown of its sheet structure, dehydroxylation, and the recombination of silica and alumina (Ptáček et al. 2014). The heating rate strongly influences these transformations, which affect the specific surface area and reactivity of metakaolinite. Thermal treatment of illite and smectite also induces structural changes that influence their pozzolanic activity, though less than in kaolinite (Fernandez et al. 2011; Garg and Skibsted 2016). Upon calcination, smectite undergoes dehydroxylation leading to partial structural breakdown and the loss of swelling capacity (Derkowski and Kuligiewicz 2022). In clays that contain significant amounts of calcite, the calcination process promotes the formation of a glassy phase, which enhances pozzolanic reactivity Danner et al. (2020).

The specific surface area of clay-based materials is closely linked to their initial phase composition and grain characteristics, which determine the functional properties of the final product. However, few studies have examined how the specific surface area evolves with firing temperature, highlighting a gap in current research and the originality of this study.

## 1. Experimental

### 1.1. Materials investigated

Ten clay raw materials from active open pits in Poland were selected to study the relationship between phase composition, specific surface area, and pozzolanic activity (Figure 3). These included ceramic clays, bentonites, weathered basalts, and red and green clays. Samples of 2–5 kg were obtained from 25 kg batches by quartering, dried at 40°C, homogenized, and stored in labelled airtight containers.

The selection aimed to maximize the diversity of clay and accessory minerals, particularly those rich in calcium and iron. Samples 1 and 2 originate from the same deposit, with sample 2 depleted in calcite. Coarse-grained marl was removed by sieving and sedimentation. Similarly, samples 9 and 10 come from different levels of one deposit – the upper (red) and middle (green) layers – differing in color and mineral composition. This sampling


Fig. 3. Location of the clay deposits from which samples were taken for testing
1) CERABUD – ground clay (Radoszyce, Świętokrzyskie Voivodeship); 2) CERABUD – ground ceramic clay (Radoszyce, Świętokrzyskie Voivodeship); 3) Bentonite (Drugnia Rządowa Limestone Mine, Świętokrzyskie Voivodeship); 4) BZMO – clay raw material (Czerwona Woda, Lower Silesia Voivodeship); 5) Rakszawa Mine – clay raw material (Rakszawa, Podkarpackie Voivodeship); 6) Wysoczany Mine – clay raw material (Wysoczany Voivodeship, Subcarpathia); 7) KOSD Rutki-Ligota. Basalt Mine – clay raw material (Tyłowice, Niemodlin, Opole Voivodeship); 8) KOSD Rutki-Ligota. Basalt Mine – weathered basalt (Tyłowice, Niemodlin, Opole Voivodeship); 9) Dylągówka-Zapady – red clay material (Dylągówka, Podkarpackie Voivodeship); 10) Dylągówka-Zapady – green clay material (Dylągówka, Podkarpackie Voivodeship)

Rys. 3. Lokalizacja złóż gliny, z których pobrano próbki do badań

approach ensured representation of both inter- and intra-deposit variability, allowing reliable assessment of how phase composition influences clay reactivity and functional properties.

### 1.2. X-ray diffraction (XRD)

X-ray diffraction (XRD) analysis was used as the standard method to assess the phase composition of the studied clay raw materials. Measurements were carried out using a Philips X'Pert Pro diffractometer with CuKα radiation and a scanning rate of 1.2°/min. The analysis was conducted over the angular range commonly applied in clay mineral studies, from 3° to 70° 2θ. Qualitative identification of the mineral components in the samples was performed using the HighScore Plus software, with reference to the JCPDS – ICDD database (Joint Committee for Powder Diffraction Standards – International Centre for Diffraction

Data). Due to the structural similarity of clay minerals and the fact that their identification is primarily based on the first, low-angle diffraction peak corresponding to the $d_{001}$ basal spacing, the analysis was further confirmed using the method of Brindley and Brown (Brindley and Brown 1980). It involved additional XRD measurements of samples saturated with ethylene glycol and after calcination at 560°C.

### 1.3. Particle size distribution

Particle size distribution was determined using a Mastersizer 2000 laser diffraction analyzer. The instrument measured light scattering by particles in suspension to calculate size and distribution within the 0.02–2 µm range, at detection angles of 0.02°–140° and a 1 Hz acquisition frequency. The suspension was prepared by mixing the sample with distilled water and seven drops of the dispersing agent Dispex, followed by 3 minutes of ultrasonic treatment to ensure proper dispersion.

### 1.4. Chemical analysis

The chemical composition of the studied materials was determined using wavelength-dispersive X-ray fluorescence (WDXRF) analysis. Measurements were performed with an Axios mAX spectrometer (PANalytical) equipped with a 4 kW Rhodium (Rh) X-ray tube. The samples were prepared in the form of pellets: a mixture of 2 g of sample and 2 g of binder was thoroughly homogenized and then pressed into disks approximately 3.5 cm in diameter.

### 1.5. Specific surface area (BET)

The specific surface area was determined using gas physical adsorption. Measurements were carried out with a Nova 1200e instrument (Quantachrome Instruments), applying the five-point BET method to calculate the surface area. Nitrogen was used as the adsorbate, and the adsorption isotherm was measured over a relative pressure range of 0.02–0.2. Prior to measurement, the samples were degassed at 100°C for 6 hours (heating rate 6 K/min).

### 1.6. Pozzolanic activity

Pozzolanic activity of studied samples was determined according to ASTM C379-65 T (1965). Following this methodology, the contents of NaOH-soluble forms of silicon oxide ($SiO_2$), aluminum oxide ($Al_2O_3$), and iron oxide ($Fe_2O_3$) were measured, which are

considered potentially reactive with $Ca(OH)_2$. Prior to analysis, all samples were calcined at 700°C for 20 minutes. This treatment aimed to activate the clay minerals, particularly kaolinite, through dehydroxylation and thermal decomposition into pozzolanically active phases (metakaolinite and amorphous silica).

## 2. Results and discussion

### 2.1. Phase composition analysis by X-ray diffraction (XRD)

Based on qualitative X-ray analysis (Figure 4), the studied samples contained clay minerals such as illite, kaolinite, smectite, chlorite, and halloysite, accompanied by non-clay phases including quartz, calcite, feldspar, and zeolite. All samples exhibited a dominant dioctahedral structure (060 reflection at 1.50 Å), while samples 4 and 7 showed reflections near 1.54 Å, indicating trioctahedral forms (Reynolds and Moore 1989).

Illite was determined in all samples except 3, characterized by reflections $d_{001} \approx 10$ Å ($2\Theta CuK\alpha \approx 8.9°$), and $d_{002} \approx 5$ Å ($2\Theta CuK\alpha \approx 17.8°$) (Brindley and Brown 1980; Reynolds and Moore 1989), with the highest amounts in samples 1, 2, and 9. Additionally, halloysite was detected in sample 8. The $d_{001}$ reflection of halloysite (10.1 Å) can be confused with

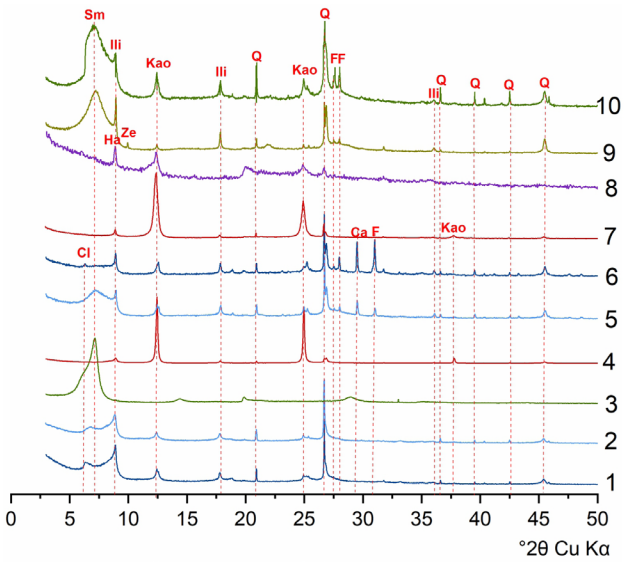


Fig. 4. XRD diagrams of samples 1–10;
Sm – Smectite, Cl – Chlorite, Kao – Kaolinite, Ili – Illite, Q – Quartz, Ha – Halloysite, Ca – Calcite, F – Feldspar, Ze – zeolite (clinoptilolite)

Rys. 4. Wykresy XRD próbek 1–10

illite (10.0 Å). After calcination at 560°C, the reflection at d ≈ 7.15 Å disappeared, indicating the dehydroxylation of kaolin-group minerals (Joussein et al. 2005; Wyszomirski et al. 2024). The presence of halloysite was also inferred from the atypical asymmetry of the $d_{001}$ reflection ≈ 7.15 Å (2ΘCuKα ≈ 12.4°). Kaolinite occurred in nine samples (absent in 3), with the highest content in 4 and 7, indicated by reflections at $d_{001}$ ≈ 7.15 Å (2ΘCuKα ≈ 12.4°), $d_{002}$ ≈ 3.57 Å (2ΘCuKα ≈ 24.9°) and $d_{003}$ ≈ 2.38 Å (2ΘCuKα ≈ 37.7°) (Reynolds and Moore 1989; Chipera and Bish 2001).

Smectite appeared in samples 3, 5, 9, and 10 – $d_{001}$ ≈ 12.5 Å reflection (2ΘCuKα ≈ 7.1°) (Brindley and Brown 1980), most abundant in sample 3. Reflections at $d_{001}$ ≈ 14 Å (2ΘCuKα ≈ 6.3°) in samples 1 and 6 (Reynolds and Moore 1989) suggest the presence of phases such as chlorite and vermiculite, confirmed by the Brindley and Brown method (1980). These are likely mixed-layer chlorite–smectite structures. Vermiculite is challenging to distinguish in the presence of smectite or chlorite due to overlapping broad bands in standard analysis (Brindley and Brown 1980).

Quartz was determined in samples 1, 2, 5, 6, 7, 9, and 10 ($d_{101}$ ≈ 3.34 Å (2ΘCuKα ≈ 26.6°); $d_{100}$ ≈ 4.26 Å (2ΘCuKα ≈ 20.8°), with the strongest peaks in 1 and 2. Calcite occurred in 5 and 6 $d_{104}$ ≈ 3.03 Å reflection (2ΘCuKα ≈ 29.4°), while feldspars – probably orthoclase – were present in 5, 6, 9, and 10 $d_{002}$ ≈ 3.24 Å (2ΘCuKα ≈ 27.5°) and $d_{040}$ ≈ 3.18 Å (2ΘCuKα ≈ 28.1°) reflections (Carroll 1970).

Samples 9 and 10 may also contain opal-A, previously reported in related studies (Panna et al. 2014). Zeolite (clinoptilolite) was identified in sample 9 $d_{001}$ ≈ 8.9 Å (2ΘCuKα ≈ 9.9°) (Pabis-Mazgaj et al. 2021). The Carpathian Flysch region of southeastern Poland, including the Dylągówka area (Franus et al. 2000; Panna et al. 2014), is known for deposits rich in smectite, zeolite, and silicate minerals, from which sample 9 was obtained.

### 2.2. Determination of particle size distribution

Granulometric analysis indicated significant variation in fine fractions (<1 µm and <2 µm), indicating the presence of clay components and potential reactivity. Clay minerals typically have particle sizes below 2 µm (Tan et al. 2017; Chen et al. 2020). Illite and fine-grained kaolinite D are concentrated in the 0.1–2 µm range, while smectite occurs mainly below 1 µm (Stoch and Sikora 1971). Kaolinite can also occur as coarse-grained kaolinite Tc, with grains up to 30 µm (Stoch and Sikora 1971; Lech and Wyszomirski 2020).

Particle size distribution is presented with cumulative (blue) and frequency (red) curves (Figure 5). SSamples 1, 2, and 9 show the highest <2 µm content (~26–34%), indicating abundant clay minerals, particularly in sample 2 (~12% <1 µm), consistent with the presence of fine-grained illite and kaolinite D, and in sample 9 with the presence of smectite (Stoch and Sikora 1971). High <10 µm (~77–92%) and <30 µm (~94–99%) fractions indicate dominance of fine-grained material with high reactivity (Kumari and Mohan 2021), supported by XRD-detected illite, smectite, and kaolinite.

Samples 3, 4, and 10 have lower <2 µm (~12–14%) and <10 µm (~44–47%) fractions. Smectite occurs in 3 and 10 despite low <1 µm content (~4%), while sample 4's low <30 µm fraction (~56%) suggests coarse-grained kaolinite Tc (Tan et al. 2017). In addition, smectite's strong aggregation of grains may be responsible for this value (Panna et al. 2014).

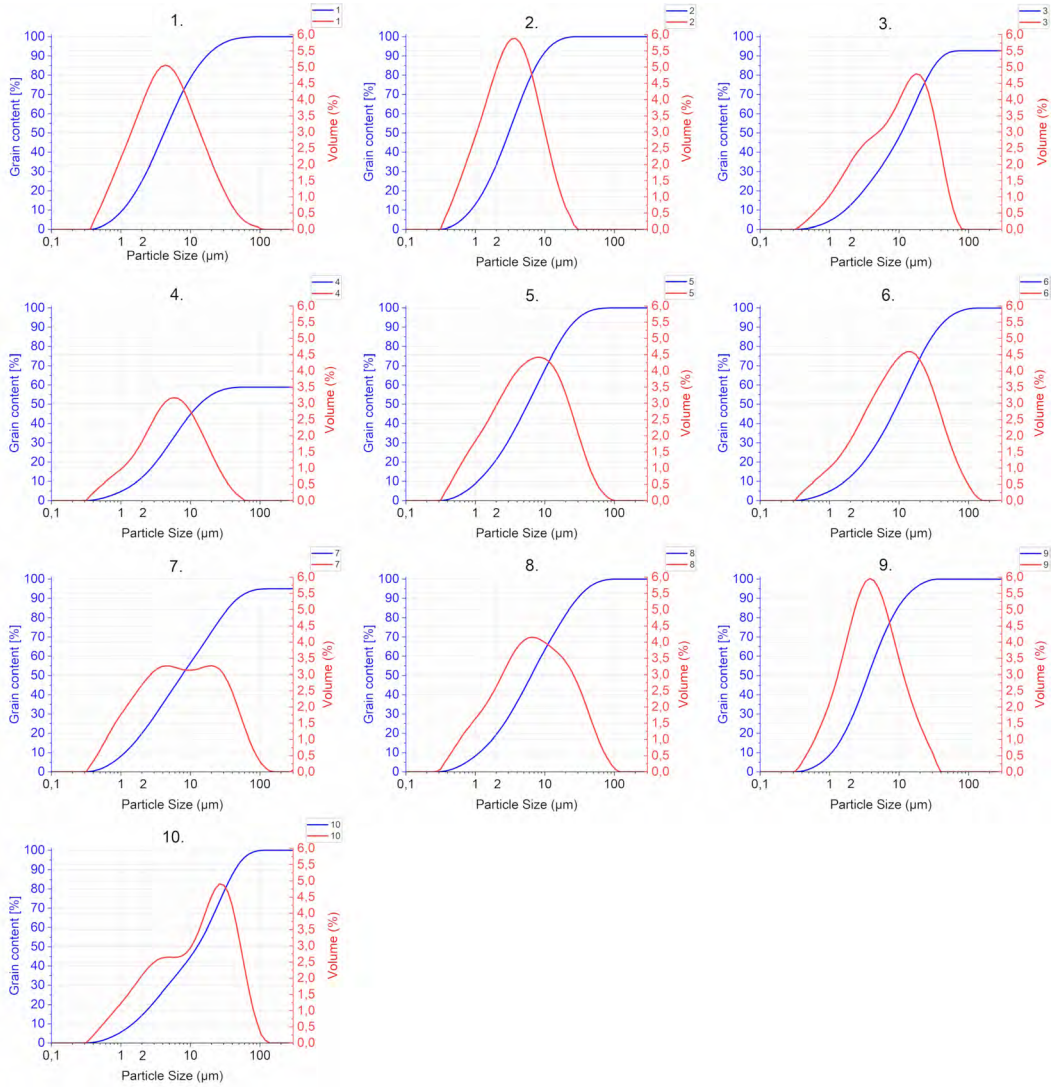


Fig. 5. Analysis of the grain size distribution of cumulative (blue lines) and frequency (red lines) curves of samples 1–10

Rys. 5. Analiza rozkładu wielkości ziaren na podstawie krzywych kumulacyjnych (niebieskie linie) i częstotliwościowych (czerwone linie) próbek 1–10

Samples 5–8 are intermediate, with <2 µm fractions of ~19–21% and <1 µm ~5–8%. XRD confirmed illite and kaolinite in all, with smectite in 5 and 9. High <10 µm (~51–67%) and <30 µm (~82–88%) fractions indicate silt–clay dominance, with sample 6 showing possible bimodality (clay plus coarser quartz, feldspar, calcite) (Stoch and Sikora 1971). Samples 7 and 8, containing illite, kaolinite, and halloysite (8), have <2 µm fractions of ~19–20% and significant <30 µm content (~82–86%), suggesting kaolinite occurs in both fine- and coarse-grained forms.

## 2.3. Chemical composition analysis

The chemical composition showed $SiO_2$, $Al_2O_3$, and $Fe_2O_3$ in all samples (Tabela 1), with variable contents of other oxides and loss on ignition (LOI), confirming phase composition diversity (Figure 4). Samples 1 and 2 come from the same deposit, but sample 2 lacks marl, reflected in lower CaO. Low LOI and high $K_2O$ indicate illite predominance. Illite contains strongly bound interlayer $K^+$, which prevents interlayer hydration; therefore, its LOI is primarily due to dehydroxylation. Sample 3 shows high MgO (3.7%) and LOI (23.8%), indicating smectite dominance due to Mg content and interlayer water (Schulze 2005; Derkowski and Kuligiewicz 2022). Samples 4 and 7 contain kaolinite, indicated by high $Al_2O_3$ contents (25.6% and 28.2%). Kaolinite shows low LOI (8.7% and 7.5%).

Table 1. Chemical analysis (% by weight) of the main and minor components

Tabela 1. Analiza chemiczna (w % masy) głównych i drugorzędnych składników

| Sample | $SiO_2$ | $Al_2O_3$ | $Fe_2O_3$ | MgO | CaO | $TiO_2$ | $K_2O$ | $Na_2O$ | MnO | $P_2O_5$ | $SO_3$ | LOI* |
|---|---|---|---|---|---|---|---|---|---|---|---|---|
| 1 | 55.3 | 17.3 | 7.5 | 2.8 | 2.2 | 1.8 | 4.5 | 0.5 | 0.2 | 0.2 | 0.0 | 7.6 |
| 2 | 57.2 | 17.9 | 7.8 | 2.3 | 0.9 | 1.7 | 4.5 | 0.2 | 0.1 | 0.1 | 0.0 | 7.3 |
| 3 | 47.5 | 14.5 | 2.0 | 3.7 | 7.5 | 0.7 | 0.1 | 0.1 | 0.0 | 0.1 | 0.0 | 23.8 |
| 4 | 57.1 | 25.6 | 1.0 | 2.0 | 0.4 | 1.7 | 3.3 | 0.2 | 0.0 | 0.1 | 0.0 | 8.7 |
| 5 | 46.9 | 13.2 | 5.5 | 2.0 | 14.4 | 2.0 | 4.3 | 0.4 | 0.3 | 0.2 | 0.1 | 10.7 |
| 6 | 43.4 | 14.0 | 5.9 | 3.1 | 15.4 | 2.6 | 4.6 | 0.6 | 0.2 | 0.2 | 1.7 | 8.4 |
| 7 | 54.4 | 28.2 | 5.8 | 0.6 | 0.3 | 1.5 | 1.4 | 0.1 | 0.0 | 0.2 | 0.1 | 7.5 |
| 8 | 24.3 | 18.0 | 26.1 | 0.6 | 0.8 | 9.0 | 0.2 | 0.1 | 0.2 | 0.6 | 0.0 | 20.0 |
| 9 | 67.1 | 12.1 | 1.6 | 3.4 | 1.8 | 1.8 | 4.0 | 0.2 | 1.6 | 0.1 | 0.0 | 6.4 |
| 10 | 66.0 | 10.5 | 3.2 | 1.5 | 1.0 | 1.8 | 3.6 | 0.6 | 0.4 | 0.2 | 0.1 | 11.1 |

* Loss on ignition.

The observed mass loss corresponds mainly to dehydroxylation of structural hydroxyl groups (Schulze 2005; Kumari and Mohan 2021). Samples 5 and 6 contain significant CaO (~14%) from calcite, with relatively low LOI and high $K_2O$, indicating a high illite proportion like samples 1 and 2. Sample 8 shows high $Fe_2O_3$ (26.1%) and $TiO_2$ (9.0%) typical of weathered basalt, low $SiO_2$ (24.3%), and LOI 20%, associated with halloysite, whose 1:1 layer includes hydration water (Schulze 2005; Wyszomirski et al. 2024). Samples 9 and 10 have the highest $SiO_2$ (67.1% and 66.0%), likely from opal-A. Sample 9's significant $K_2O$ reflects the presence of illite and zeolite (clinoptilolite) (Panna et al. 2014).

## 2.4. Specific surface area analysis (BET)

BET surface area measurements (Tabela 2; Figure 6) showed values ranging from 16.1 to 95.2 $m^2/g$, primarily dependent on the dominant clay mineral. The highest surface area was observed for halloysite-rich sample 8, which is consistent with previous observations (Wyszomirski et al. 2024), while smectite-containing samples 3, 9, and 10 ranged from 52.1 to 64.1 $m^2/g$, as also reported in earlier studies (Panna et al. 2014, 2025). The lowest values occurred in kaolinite-rich samples 4, 7, and clay minerals-poor sample 6, as also reported by Ikegami et al. (2025). Tubular halloysite exhibits the largest specific surface, expandable smectites intermediate, and non-expanding illite and kaolinite the lowest. Firing at 700°C caused minor surface area loss in kaolinite-bearing samples (sample 4: 10.43%; 7: 15.35%) due to structural stability upon dehydroxylation to metakaolinite, with the minimal surface area loss compared to the pre-firing state related to the loss of hydroxyl groups (Bellotto et al. 1995; Fernandez et al. 2011). In contrast, smectite- and illite-rich samples showed larger reductions. They lose interlayer water – its amount depends on the charge of the layers and the type of interlayers cation – and dehydroxylates, leading to structural collapse (smoothing the layers surface) and, in consequence, decreased surface area (Schulze 2005; Ikegami et al. 2025).

Table 2. Results of specific surface area determinations ($m^2/g$) of samples 1–10

Tabela 2. Wyniki oznaczeń powierzchni właściwej ($m^2/g$) próbek 1–10

| Temperature (°C) | 1 | 2 | 3 | 4 | 5 | 6 | 7 | 8 | 9 | 10 |
|---|---|---|---|---|---|---|---|---|---|---|
| 21 | 37.2 | 35.3 | 52.1 | 16.3 | 36.7 | 16.1 | 20.2 | 95.2 | 63.1 | 64.1 |
| 700 | 27.6 | 23.0 | 22.9 | 14.6 | 16.0 | 8.1 | 17.1 | 66.7 | 48.4 | 48.0 |
| 850 | 10.8 | 14.7 | 12.5 | 14.5 | 7.1 | 5.4 | 15.8 | 31 | 18.7 | 17.0 |
| 900 | 3.9 | 3.9 | 3.2 | 14.1 | 3.5 | 2.4 | 15.5 | 23.7 | 16.0 | 7.6 |
| 950 | 1.8 | 1.9 | 0.7 | 11.7 | 3.3 | 1.9 | 12.5 | 19.6 | 10.1 | 3.7 |

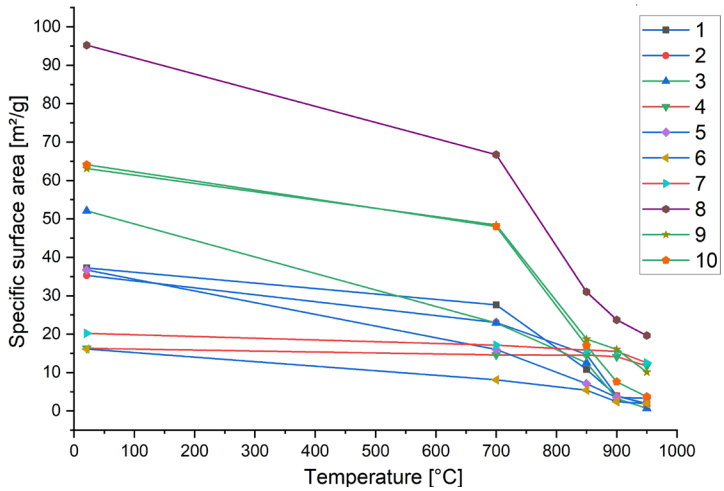


Fig. 6. Summary of specific surface area measurements depending on the firing temperature of 10 samples. The color of the lines depends on the predominant clay mineral: red line – kaolinite; blue line – illite; green line – smectite; purple line – halloysite

Rys. 6. Podsumowanie wyników pomiarów powierzchni właściwej w zależności od temperatury wypalania dla 10 próbek. Kolor linii zależy od dominującego minerału ilastego: czerwona linia – kaolinit; niebieska linia – illit; zielona linia – smektyt; fioletowa linia – halloizyt

Further surface area decreases at 850–950°C are attributed to fluxing agents ($K_2O$, $Na_2O$, CaO, MgO, $TiO_2$, $Fe_2O_3$), which accelerate densification and pore closure (Dey et al. 2018). Samples 4 and 7, with the lowest flux content, showed the lowest reduction (19.9% and 26.9%) in the 700–950°C range.

## 2.5. Assessment of pozzolanic activity

Pozzolanic activity analysis (Tabela 3) showed the highest values at 700°C for samples 7 (36.14%), 10 (35.19%), 4 (33.43%), and 3 (31.64%), reflecting effective thermal activation of kaolinite (samples 4 and 7), smectite (3 and 10), and reactive silica (opal-A in 10) (Czapik and Cebulski 2018). Activity in 4 and 7 is linked to metakaolinite formation via dehydroxylation. Smectite-rich samples 3 and 10 also exhibited high activity, consistent with reports that Na- and Ca-montmorillonites gain reactivity after dehydroxylation (Garg and Skibsted 2014). Amorphous silica (opal-A) further enhances CaO fixation, explaining sample 10's higher activity compared to 3 (Li et al. 2022).

Minor contributions from $Fe_2O_3$ (~0.44–0.46%) in samples 7 and 8 may result from $Fe^{3+}$ substitution in kaolinite octahedral layers, causing lattice distortions even at ~0.5% $Fe_2O_3$ (Mestdagh et al. 2018). Lowest activity occurred in samples 6 (7.69%), 2 (10.23%), and 5 (11.32%) due to low kaolinite and smectite content and high non-clay mineral proportion.

Thermally activated smectites and illites exhibit reactivity controlled by tetrahedral sheet accessibility in the 2:1 layered structure. Dehydroxylation induces amorphization of the tetrahedral sheet, disrupting the long-range structural order of the layered aluminosilicate. The resulting disordered phase exposes highly reactive sites that readily react with $Ca(OH)_2$ to form secondary hydration products (Garg and Skibsted 2016). This mechanism applies to kaolinite, smectite, and illite, with tetrahedral sheets on calcined outer layers likely responsible for initiating pozzolanic reactions. These data do not explicitly confirm that the tetrahedral sheets on the outer surfaces of 2:1 layers are the source of reactivity and pozzolanic mechanisms. But this allows the hypothesis that these layers, being the most accessible after calcination, are primarily responsible for initiating the reaction with lime. This is also confirmed by the low values of pozzolanic activity derived from $Al_2O_3$ in samples rich in 2:1 clay minerals.

Table 3. Results of determining the pozzolanic activity of samples calcined at 700°C

Tabela 3. Wyniki oznaczenia aktywności pucolanowej próbek kalcynowanych w temperaturze 700°C

| Sample | Pozzolanic active oxides (% by weight) | | | |
|---|---|---|---|---|
| | $SiO_2$ | $Al_2O_3$ | $Fe_2O_3$ | total active oxides |
| 1 | 10.26 | 3.24 | 0.00 | 13.50 |
| 2 | 7.26 | 2.97 | 0.00 | 10.23 |
| 3 | 23.83 | 7.81 | 0.00 | 31.64 |
| 4 | 18.54 | 14.89 | 0.00 | 33.43 |
| 5 | 8.34 | 2.98 | 0.00 | 11.32 |
| 6 | 5.98 | 1.71 | 0.00 | 7.69 |
| 7 | 20.14 | 15.56 | 0.44 | 36.14 |
| 8 | 16.31 | 11.61 | 0.46 | 28.38 |
| 9 | 10.98 | 2.05 | 0.00 | 13.03 |
| 10 | 33.46 | 1.73 | 0.00 | 35.19 |

## Summary and conclusion

1. Pozzolanic reactivity depends primarily on mineral composition and its response to thermal activation. Kaolinite transforms into metakaolinite through dehydroxylation and structural disordering of the octahedral sheet, producing aluminosilicate phases capable of binding $Ca(OH)_2$ and exhibiting the highest pozzolanic reactivity.

2. Firing at around 700°C causes only a slight decrease in BET surface area in kaolinite-bearing materials, indicating that metakaolinite remains structurally stable and that the reduction mainly results from hydroxyl loss, which smooths the surface of the octahedral layers. Although increased BET surface area often correlates with higher reactivity – since fine particles and structural disorder enlarge the reactive surface – kaolinite exhibits the highest activity despite its lower BET, demonstrating that mineralogical transformation can outweigh surface area alone.
3. Smectite- and illite-rich clays show stronger BET surface-area reductions upon firing. The loss of interlayer water (the magnitude depending on layer charge and interlayer cation) together with dehydroxylation promotes structural collapse and surface smoothing, thus decreasing surface area. At the same time, dehydroxylation-induced amorphization of $SiO_4$ tetrahedra generates reactive sites that can bind $Ca(OH)_2$. Therefore, the reactivity of 2:1 clays is governed by the accessibility of the tetrahedral sheet after activation.
4. Further surface-area reduction at 850–950°C occurs due to the action of fluxing oxides ($K_2O$, $Na_2O$, CaO, MgO, $TiO_2$, $Fe_2O_3$), which enhance sintering and close pores. Although the present study assessed pozzolanic activity only for the material calcined at 700°C, the chemical composition indicates that clays containing flux oxides may exhibit enhanced sintering at higher firing temperatures, which can indirectly influence their reactivity.
5. The presence of amorphous silica (opal-A) enhances CaO fixation and can increase pozzolanic performance in some smectite-rich materials, accounting for inter-sample activity differences among otherwise similar 2:1 clays. Although kaolinite remains the most reliable source of reactive phase for SCMs, smectite-rich clays can also serve as viable alternatives when thermal activation and milling ensure accessibility of reactive tetrahedral layers, maintain appropriate particle size, and limit flux-induced densification during firing. Their activity is attributed to dehydroxylation and amorphization of the 2:1 tetrahedral layers, providing reactive silica, and fine particle size increasing surface area.
6. Robust prediction of pozzolanic potential requires integrated datasets: detailed mineralogy, thermal behavior, particle-size distribution, and BET.

*Research project supported by the program "Excellence Initiative – Research University" at the AGH University of Krakow, project no. 10388.*

*The Authors have no conflict of interest to declare.*

## REFERENCES

Amiri et al. 2022 – Amiri, I., Haddad, A. and Jafarian, Y. 2022. Evaluation of mechanical properties of cement and zeolite-stabilized sand using monotonic simple shear test. *Journal of Civil and Environmental Engineering* 52(107), pp. 15–25, https://doi.org/10.22034/jcee.2020.39108.1931.

ASTM 1965 – ASTM C379-65T 'Fly Ash Use as Pozzolanic Material with Lime'. American Society for Testing and Materials.

Ayari et al. 2007 – Ayari, F., Srasra, E. and Trabelsi Ayadi, M. 2007. Effect of exchangeable cations on the physicochemical properties of smectite. *Surface Engineering and Applied Electrochemistry* 43(5), pp. 369–378, https://doi.org/10.3103/S1068375507050110.

Bellotto et al. 1995 – Bellotto, M., Gualtieri, A., Artioli, A. and Clark, S.M. 1995. Kinetic study of the kaolinite–mullite reaction sequence. Part I: Kaolinite dehydroxylation. *Physics and Chemistry of Minerals* 22, pp. 207–217, https://doi.org/10.1007/BF00202253.

Bergaya, F. and Lagaly, G. 2013. General introduction: Clays, clay minerals, and clay science. *Handbook of Clay Science, Developments in Clay Science* 5, pp. 21–81, https://doi.org/10.1016/B978-0-08-098258-8.00001-8.

Brigatti et al. 2013 – Brigatti, M.F., Galán, E. and Theng, B.K.G. 2013. Structure and mineralogy of clay minerals. *Handbook of Clay Science, Developments in Clay Science* 5, pp. 21–81, https://doi.org/10.1016/B978-0-08-098258-8.00002-X.

Brindley, G.W. and Brown, G. 1980. *X-ray diffraction procedures for clay mineral identification*. [In:] Brindley, G.W. and Brown, G. (eds) *Crystal Structures of Clay Minerals and Their X-Ray Identification, Mineralogical Society*, London, pp. 305–356.

Carroll, D. 1970. Clay Minerals: A Guide to Their X-ray Identification. *Geological Society of America.* Spec. Pap., 126.

Chen et al. 2020 – Chen, L., Jin, X., Chen, H., He, Z., Qiu, L. and Duan, H. 2020. Grain size distribution and clay mineral distinction of rare earth ore through different methods. *Minerals* 10(4), https://doi.org/10.3390/min10040353.

Chipera, S.J. and Bish, D.L. 2001. Baseline studies of the Clay Minerals Society source clays: powder X-ray diffraction analyses. *Clays and Clay Minerals* 49(5), pp. 398–409, https://doi.org/10.1346/CCMN.2001.0490507.

Czapik, P. and Cebulski, M. 2018. The properties of cement mortar with natural zeolite and silica fume additions. *Structure and Environment* 10(2), pp. 105–113, https://doi.org/10.30540/sae-2018-010.

Danner et al. 2020 – Danner, T., Norden, T. and Justnes, H. 2020. *The effect of calcite in the raw clay on the pozzolanic activity of calcined illite and smectite.* [In:] Martirena, F., Scrivener, K.L. and Fabbri, B. (eds) *Calcined Clays for Sustainable Concrete, RILEM Bookseries*, Springer, pp. 139–146.

Daou et al. 2023 – Daou, I., Mocuta, C., Lecomte-Nana, G.L., Tessier-Doyen, N., Peyratout, C., Guinebretière, R. and Thiaudière, D. 2023. Dehydroxylation of kaolinite and halloysite-rich samples: an in situ study of the texture and structural evolutions. *Minerals* 13(11), https://doi.org/10.3390/min13111418.

Derkowski, A. and Kuligiewicz, A. 2022. Thermal analysis and thermal reactions of smectites: a review of methodology, mechanisms, and kinetics. *Clays and Clay Minerals* 70, pp. 946–972, https://doi.org/10.1007/s42860-023-00222-y.

Dey et al. 2018 – Dey, S., Ray, D., Mondal, A. and Parya, T.K. 2018. Effect of yttria on sintering and microstructural behavior of reaction sintered mullite based on bauxite, fly ash and precipitated silica. *Ceramics International* 44(9), pp. 10087–10093, https://doi.org/10.1016/j.ceramint.2018.02.214.

Dogan et al. 2006 – Dogan, A.U., Dogan, M., Onal, M., Sarikaya, Y., Aburub, A. and Wurster, D.E. 2006. Baseline studies of the Clay Minerals Society source clays: specific surface area by the Brunauer–Emmett–Teller (BET) method. *Clays and Clay Minerals* 54(1), pp. 62–66, https://doi.org/10.1346/CCMN.2006.0540108.

Dogan et al. 2007 – Dogan, M., Dogan, A.U., Yesilyurt, F.I., Alaygut, D., Buckner, I. and Wurster, D.E. 2007. Baseline studies of the Clay Minerals Society special clays: specific surface area by the Brunauer–Emmett–Teller (BET) method. *Clays and Clay Minerals* 55, pp. 534–541, https://doi.org/10.1346/CCMN.2007.0550508.

Dondi et al. 1998 – Dondi, M., Fabbri, B. and Guarini, G. 1998. Specific surface of clay raw materials used in the Italian ceramic industry. *Industrial Ceramics* 18(3).

Fernnandez et al. 2011 – Fernandez, R., Martirena, F. and Scrivener, K.L. 2011. The origin of the pozzolanic activity of calcined clay minerals: a comparison between kaolinite, illite and montmorillonite. *Cement and Concrete Research* 41(1), pp. 113–122, https://doi.org/10.1016/j.cemconres.2010.09.013.

Franus et al. 2000 – Franus, W., Manecki, A. and Wieser, T. 2000. Rancieite from clinoptilolite-montmorillonite claystones of the Scole Unit (the Polish Flysch Carpathians). *Mineralogia Polonica* 32(1), pp. 48–59.

Garg, N. and Skibsted, J. 2014. Thermal activation of a pure montmorillonite clay and its reactivity in cementitious systems. *The Journal of Physical Chemistry C* 118(21), pp. 11464–11476, https://doi.org/10.1021/jp502529d.

Garg, N. and Skibsted, J. 2016. Pozzolanic reactivity of a calcined interstratified illite/smectite (70/30) clay. *Cement and Concrete Research*. 79, pp. 101–111, https://doi.org/10.1016/j.cemconres.2015.08.006.

Hollanders, S. 2017. Mineralogical study of the pozzolanic properties of calcined clays. *Ph.D. thesis, Arenberg Doctoral School, Faculty of Science.*

Ikegami et al. 2025 – Ikegami, M., Fukutani, S. and Yoneda, M. 2025. Characteristic changes of calcined clay minerals as heavy metal adsorbents. *Clay Minerals* 60(1), pp. 60–68, https://doi.org/10.1180/clm.2025.3.

Irawan, S. and Samsuri, A. 2006. Mineralogy and physico-chemical characteristics of bentonite clay from Sabah, Malaysia. *Environmental Science: Indian Journall* 1(1), pp. 16–23.

Joussein et al. 2005 – Joussein, E., Petit, S., Churchman, J., Theng, B.K.G., Righi, D.P. and Delvaux, B. 2005. Halloysite clay minerals – a review. *Clay Minerals* 40(4), pp. 383–426, https://doi.org/10.1180/0009855054040180.

Kakali et al. 2001 – Kakali, G., Perraki, T., Tsivilis, S. and Badogiannis, E. 2001. Thermal treatment of kaolin: the effect of mineralogy on the pozzolanic activity. *Applied Clay Science* 20(1–2), pp. 73–80, https://doi.org/10.1016/S0169-1317(01)00040-0.

Kaufhold et al. 2010 – Kaufhold, S., Dohrmann, R., Klinkenberg, M., Siegesmund, S. and Ufer, K. 2010. $N_2$-BET specific surface area of bentonites. *Journal of Colloid and Interface Science* 349(1), pp. 275–282, https://doi.org/10.1016/j.jcis.2010.05.018.

Koch, D. 2002. Bentonites as a basic material for technical base liners and site encapsulation cut-off walls. *Applied Clay Science* 21, pp. 1–11, https://doi.org/10.1016/S0169-1317(01)00087-4.

Kuila, U. and Prasad, M. 2013. Specific surface area and pore-size distribution in clays and shales. *Geophysical Prospecting* 61(2), pp. 196–196, https://doi.org/10.1111/1365-2478.12028.

Kumari, N and Mohan, C. 2021. *Basics of clay minerals and their characteristic properties.* [In:] Morari Do Nascimento G (ed.) *Clay and Clay Minerals.* IntechOpen, https://doi.org/10.5772/intechopen.97672.

Lech, R. and Wyszomirski, P. 2020. Methods of calcining kaolin raw materials in the production of metakaolin. *Materiały Ceramiczne/Ceramic Materials* 72(1), pp. 33–48.

Li et al. 2022 – Li, W., Jiang, C., Zhang, Q. and Li, S. 2022. Evaluation of pozzolanic and alkali-activated reactivity of low-purity calcium bentonite. *Materials* 15(22), https://doi.org/10.3390/ma15228015.

Liu et al. 2021 – Liu, Y., Huang, Q., Zhao, L. and Lei, S. 2021. Influence of kaolinite crystallinity and calcination conditions on the pozzolanic activity of metakaolin. *Gospodarka Surowcami Mineralnymi – Mineral Resources Management* 37(1), pp. 39–56, https://doi.org/10.24425/gsm.2021.136295.

Mestdagh et al. 2018 – Mestdagh, M.M., Derluyn, H., Mertens, G. and Elsen, J. 2018. Iron in kaolinite: II. The relationship between kaolinite crystallinity and iron content. *Clay Minerals* 53(2), pp. 167–178, https://doi.org/10.1017/claymin.1980.015.1.01.

Murray, H.H. 2006. *Structure and composition of the clay minerals and their physical and chemical properties.* Chapter 2 [In:] *Applied Clay Mineralogy*, *Developments in Clay Science,* Vol. 2.

Pabis-Mazgaj et al. 2021 – Pabis-Mazgaj, E., Gawenda, T., Pichniarczyk, P. and Stempkowska, A. 2021. Mineral composition and structural characterization of the clinoptilolite powders obtained from zeolite-rich tuffs. *Minerals* 11(10), https://doi.org/10.3390/min11101030.

Panna et al. 2014 – Panna, W., Wyszomirski, P. and Myszka, R. 2014. Characteristics of the clayey-siliceous rock from the Dylągówka–Zapady deposit (Polish Flysch Carpathians) as a mineral raw material *Gospodarka Surowcami Mineralnymi – Mineral Resources Management* 30(2), pp. 85–102, https://doi.org/10.2478/gospo-2014-0012.

Panna et al. 2024 – Panna, W., Prewendowski, S., Juda, W. and Szumera, M. 2024. Possibilities of producing lightweight aggregates from silica clay raw material and cellulosic waste. *Journal of Thermal Analysis and Calorimetry 149*, pp. 10709–10722, https://doi.org/10.1007/s10973-024-13426-8.

Panna et al. 2025 – Panna, W., Reczyński, W., Szumera, M., Prewendowski, S. and Gajek, M. 2025. Sorption properties of selected clays from south-eastern Poland and their prospects for use in environmental protection. *Gospodarka Surowcami Mineralnymi – Mineral Resources Management* 41(1), pp. 141–161, https://doi.org/10.24425/gsm.2025.153176.

Ptáček et al. 2014 – Ptáček, P., Frajkorová, F., Šoukal, F. and Opravil, T. 2014. Kinetics and mechanism of three stages of thermal transformation of kaolinite to metakaolinite. *Powder Technology* 264, pp. 439–445, https://doi.org/10.1016/j.powtec.2014.05.047.

Rashad, A.M. 2013. Metakaolin as cementitious material: history, sources, production and composition – a comprehensive overview. *Construction and Building Materials* 41, pp. 303–318, https://doi.org/10.1016/j.conbuildmat.2012.12.001.

Reynolds, R.C. and Moore, D.M. 1989. X-ray Diffraction and the Identification and Analysis of Clay Minerals. Oxford University Press, New York.

Schoonheydt, R. and Johnston, C. 2011. The surface properties of clay minerals. [In:] *Layered Mineral Structures and their Application in Advanced Technologies* (pp. 335–370) Chapter: 10 *The Mineralogical Society of Great Britain and Ireland*, https://doi.org/10.1180/EMU-notes.11.10.

Schulze, D.G. 2005. Clay minerals. *Encyclopedia of Soils in the Environment* 4, pp. 246–254, https://doi.org/10.1016/B0-12-348530-4/00189-2.

Snellings et al. 2012 – Snellings, R., Mertens, G. and Elsen, J. 2012. Supplementary cementitious materials. *Reviews in Mineralogy and Geochemistry* 74, pp. 211–278, https://doi.org/10.2138/rmg.2012.74.6.

Stoch, L. and Sikora, W. 1971. Typomorphic significance of grain size of clay minerals (*Typomorficzne znaczenie uziarnienia minerałów ilastych*). *Przegląd Geologiczny* 19(1), pp. 1–6 (*in Polish*).

Tan et al. 2017 – Tan, X., Liu, F., Hu, L., Reed, A.H., Furukawa, Y. and Zhang, G. 2017. Evaluation of the particle sizes of four clay minerals. *Applied Clay Science* 135, pp. 313–324, https://doi.org/10.1016/j.clay.2016.10.012.

Wang et al. 2017 – Wang, Q., Zhu, C., Yun, J. and Yang, G. 2017. Isomorphic substitutions in clay materials and adsorption of metal ions onto external surfaces: a DFT investigation. *The Journal of Physical Chemistry* C 121(48), https://doi.org/10.1021/acs.jpcc.7b03488.

Wyszomirski et al. 2024 – Wyszomirski, P., Szydłak, T., Zawadzki, T. and Baranowski, M. 2024. Basalt Weathering Crust from Rutki near Niemodlin (Opole Voivodeship) – opportunities for its current utilization and remarks on its former use. *Gospodarka Surowcami Mineralnymi – Mineral Resources Management* 40(2), pp. 69–87, https://doi.org/10.24425/gsm.2024.150822.

Xie et al. 2024 – Xie, S., Huang, L., Su, C., Yan, J., Chen, Z., Li, M., Du, M. and Zhang, H. 2024. Application of clay minerals as adsorbents for removing heavy metals from the environment. *Green and Smart Mining Engineering* 1(3), pp. 249–261, https://doi.org/10.1016/j.gsme.2024.07.002.

Zunino, F. and Scrivener, K. 2024. Reactivity of kaolinitic clays calcined in the 650°C–1050°C temperature range: towards a robust assessment of overcalcination. *Cement and Concrete Composites* 146, https://doi.org/10.1016/j.cemconcomp.2023.105380.

## POZZOLANIC REACTIVITY AND SPECIFIC SURFACE AREA OF THERMALLY TREATED CLAY MATERIALS: COMPARATIVE STUDY OF SMECTITE, ILLITE AND KAOLINITE-BASED COMPOSITIONS

Keywords

clay-based materials, thermal treatment, pozzolanic activity,
raw material characterization, supplementary cementitious materials (SCMs)

Abstract

Ten clay mineral samples from currently exploited deposits in Poland were examined to determine how mineral composition and thermal transformations affect specific surface area and pozzolanic reactivity. The raw materials exhibited wide mineralogical variability, including clays dominated by illite, smectite, kaolinite, and halloysite, along with minor crystalline phases rich in Ca, Fe, Mg, and alkalis. Phase composition and its evolution during firing were determined using X-ray diffraction (XRD), while changes in specific surface area were measured by the Brunauer–Emmett–Teller (BET) method. Pozzolanic activity was assessed through dissolution tests in alkaline solutions. Firing caused dehydroxylation, amorphization, and structural collapse of layered minerals, leading to the formation of highly reactive aluminosilicate phases. The highest reactivity was observed in materials containing

kaolinite and smectite. In kaolinite, it resulted from the formation of metakaolinite – a highly reactive pozzolanic phase. In smectite-rich materials, the activity was attributed to dehydroxylation and amorphization of the 2:1 layers and to the presence of amorphous silica (opal-A), which enhances CaO fixation. Additionally, fine particle size increased the specific surface area and accessibility of reactive tetrahedral layers. However, the results showed that surface area alone did not determine reactivity – the key factors were chemical composition and the nature of thermally transformed phases. This study elucidates the interrelations between mineralogy, microstructural evolution, and pozzolanic properties, providing insights for optimizing clay raw materials as sustainable pozzolanic additives and functional components in ceramic and environmental technologies.

## REAKTYWNOŚĆ PUCOLANOWA I POWIERZCHNIA WŁAŚCIWA TERMICZNIE OBROBIONYCH MATERIAŁÓW ILASTYCH: BADANIE PORÓWNAWCZE KOMPOZYCJI NA BAZIE SMEKTYTU, ILLITU I KAOLINITU

Słowa kluczowe

materiały ilaste, obróbka termiczna, aktywność pucolanowa,
charakterystyka surowcowa, uzupełniające materiały cementowe (SCM)

Streszczenie

Dziesięć próbek minerałów ilastych z obecnie eksploatowanych złóż w Polsce przebadano w celu określenia, w jaki sposób skład mineralny i przemiany termiczne wpływają na powierzchnię właściwą oraz reaktywność pucolanową. Surowce wykazywały szeroką zmienność mineralogiczną, obejmującą iły z dominacją illitu, smektytu, kaolinitu i haloizytu, a także mniejsze ilości faz krystalicznych bogatych w Ca, Fe, Mg i alkalia. Skład fazowy oraz jego zmiany podczas wypalania określono metodą dyfrakcji rentgenowskiej (XRD), natomiast zmiany powierzchni właściwej oznaczono metodą Brunauera–Emmetta–Tellera (BET). Aktywność pucolanową oceniono za pomocą testów rozpuszczalności w roztworach alkalicznych. Proces wypalania powodował dehydroksylację, amorfizację i załamanie struktury minerałów warstwowych, prowadząc do powstania wysoko reaktywnych faz glinokrzemianowych. Największą reaktywność wykazywały materiały zawierających kaolinit i smektyt. W przypadku kaolinitu wynikała ona z tworzenia metakaolinitu – wysoce reaktywnej fazy pucolanowej. W smektytach natomiast aktywność przypisano dehydroksylacji i amorfizacji warstw 2:1 oraz obecności amorficznej krzemionki (opal-A), sprzyjającej wiązaniu CaO. Dodatkowo drobne uziarnienie zwiększało powierzchnię właściwą i dostępność reaktywnych warstw tetraedrycznych. Wyniki wykazały jednak, że sama powierzchnia właściwa nie decyduje o reaktywności – kluczowe znaczenie mają skład chemiczny i charakter termicznie przekształconych faz. Badanie to wyjaśnia współzależności między mineralogią, ewolucją mikrostrukturalną a właściwościami pucolanowymi, dostarczając wskazówek dotyczących optymalizacji surowców ilastych jako zrównoważonych dodatków pucolanowych oraz funkcjonalnych komponentów w technologiach ceramicznych i środowiskowych.